Advanced Composite Materials
Publication details, including instructions for authors and subscription information:
http://www.tandfonline.com/loi/tacm20

Modeling of time-dependent behavior of deformation and transverse cracking in cross-ply laminates

Keiji Ogi [a] & Yoshihiro Takao [b]

[a] Department of Materials Science and Engineering, Faculty of Engineering, Ehime University, 3 Bunkyocho, Matsuyama, Ehime 790-8577, Japan

[b] Research Institute for Applied Mechanics, Kyushu University, 6-1 Kasuga-Koen, Kasuga, Fukuoka, 816-8580, Japan

Version of record first published: 02 Apr 2012.

To cite this article: Keiji Ogi & Yoshihiro Takao (2001): Modeling of time-dependent behavior of deformation and transverse cracking in cross-ply laminates , Advanced Composite Materials, 10:1, 39-62

To link to this article: http://dx.doi.org/10.1163/15685510152546358

Adv. Composite Mater., Vol. 10, No. 1, pp. 39–62 (2001)

Modeling of time-dependent behavior of deformation and transverse cracking in cross-ply laminates

KEIJI OGI [1,*] and YOSHIHIRO TAKAO [2]

[1] *Department of Materials Science and Engineering, Faculty of Engineering, Ehime University, 3 Bunkyocho, Matsuyama, Ehime 790-8577, Japan*
[2] *Research Institute for Applied Mechanics, Kyushu University, 6-1 Kasuga-Koen, Kasuga, Fukuoka, 816-8580, Japan*

Received 21 June 2000; accepted 25 September 2000

Abstract—A model is developed to predict the transverse crack density and strain response in a cross-ply laminate under monotonic, bilinear and constant loading. First, the strain response of the cross-ply laminate due to transverse cracking is presented based on the viscoelasticity theory and shear lag analysis. The transverse crack density is given as a function of both time and stress using a probabilistic failure concept. Secondly, monotonic tensile tests, bilinear tensile tests and constant load tests of cross-ply laminates are carried out to measure the strains and transverse crack density. A few parameters necessary for the probabilistic function are determined from the monotonic tensile tests at various stress rates. Finally, good agreement of strains and crack density in bilinear and constant load cases between experimental results and predictions verifies the validity of the present model.

Keywords: Transverse cracking; time-dependent behavior; shear lag analysis; probabilistic failure.

1. INTRODUCTION

Characterization of the environmental effect of polymer composites is essential because of the time-dependent behavior of polymer matrix. In addition to the viscoelastic deformation, damage in composites is expected to increase with time under mechanical loading.

Time-dependent behavior in composite materials has been studied mostly by means of a viscoelasticity theory. Lou and Shapery [1] established a nonlinear viscoelastic constitutive equation based on the thermodynamic theory. Horoschenkoff [2] applied Shapery's theory to describe the tensile creep behavior of $[90_8^\circ]$ and $[\pm 45_4^\circ]_S$ carbon/epoxy and carbon/PEEK laminates. Dillard *et al.* [3] and Dillard and Brinson [4] employed a nonlinear compliance model based on the Findley

*To whom correspondence should be addressed. E-mail: kogi@en2.ehime-u.ac.jp

power law to describe the viscoelastic response in composite laminates. Flaggs and Crossman [5] developed a constitutive model on the basis of linear viscoelasticity. Chung *et al.* [6] proposed a viscoplastic model by means of a one-parameter creep potential function.

Shear lag analysis has been employed in conjunction with statistical approaches to describe the development of transverse cracking in cross-ply laminates by many researchers. Manders *et al.* [7] investigated multiple fracture in glass/epoxy cross-ply laminates on the basis of the Weibull distribution of failure strain. Fukunaga *et al.* [8] predicted the transverse crack density using a shear lag model and statistical strength analysis. Peters [9] discussed the strength of 90° plies in cross-ply laminates based on the Weibull strength distribution. Lim and Hong [10] proposed a modified shear lag model, which satisfies more refined boundary conditions. Takeda and Ogihara [11] established a probabilistic model based on a shear lag analysis considering the constraint effect, residual thermal strains and delamination.

On the other hand, stochastic theories have been employed to predict the lifetime of fibres. Coleman [12] proposed a time-dependent Weibull distribution function (breakdown function) for the creep-rupture lifetime of polymer fibers, where its critical value is regarded as a random variable. Phoenix *et al.* [13] presented a statistical model for prediction of strength and lifetime during creep of model carbon/epoxy composites taking into account stress redistribution and creep of the matrix. Goda and Hamada [14] evaluated the life time distribution of boron fibers based on Coleman's theory [12].

Time-dependent behavior of the transverse cracking has been investigated experimentally by Moore and Dillard [15] and Raghavan and Meshii [16]. Raghavan and Meshii [16] conducted constant strain rate and constant stress tests of AS4/3501-6 cross-ply laminates and showed that the matrix crack density and its rate of increase depend on strain rate and stress, respectively. However, an analytical model to predict the crack density as a function of both time and stress has not been proposed yet.

In our previous paper [17], a creep model is developed to predict the strain response of a cross-ply laminate where the transverse crack density increases with time under a constant stress. The objective of the present study is to extend the previous theory and to apply it to not only constant loading but also monotonic and bilinear loading. First, the previous theory is slightly modified to obtain the strain response of a cross-ply laminate on transverse cracking for constant loading and linear loading. The transverse crack density is given as a function of both time and stress using the time-dependent Weibull distribution function. Secondly, monotonic tensile tests, bilinear tensile tests and constant load tests are conducted on $[0/90_3^\circ]_S$ carbon/epoxy laminates. In these tests the stress–strain behaviour and transverse crack density are measured. A set of parameters for expressing the crack density is determined from the monotonic tensile tests at four different stress rates. Finally, the crack density and the strain response in both bilinear and constant load tests are

predicted using these parameters and compared with the experimental data to verify the present model.

2. MODELING

2.1. Strain response

In order to obtain the strain response of a cross-ply laminate on transverse cracking, some assumptions are made. First, all the elastic moduli are functions of time and independent of the stress state. Secondly, no delamination occurs starting from a transverse crack tip. Thirdly, stress and strain distributions are obtained by using a modified shear lag model shown in Fig. 1 [10, 17]. Here, the interlaminar shear layer has a role of transferring the shear stress between the 0° ply and 90° ply. The residual thermal strains are assumed to be independent of time because they are in an equilibrium state. Finally, the following creep compliance and relaxation modulus matrices of a lamina are assumed:

$$\boldsymbol{S}^{(1)}(t) = \begin{bmatrix} S_{11}^0 & S_{12}^0 \\ S_{12}^0 & S_{22}^0 + p_{22}\left(1 - \mathrm{e}^{-t/T'}\right) \end{bmatrix}, \tag{1}$$

$$\boldsymbol{Q}^{(1)}(t) = \begin{bmatrix} Q_{11}^0 & Q_{12}^0 - q_{12}\left(1 - \mathrm{e}^{-t/T}\right) \\ Q_{12}^0 - q_{12}\left(1 - \mathrm{e}^{-t/T}\right) & Q_{22}^0 - q_{22}\left(1 - \mathrm{e}^{-t/T}\right) \end{bmatrix}, \tag{2}$$

where S_{ij}^0 and Q_{ij}^0 are the initial values of each component, and T, T', p_{22}, q_{22} and q_{12} are positive constants. The following relations are needed in order that $\boldsymbol{S}^{(1)}(t)\boldsymbol{Q}^{(1)}(t) = \boldsymbol{I}$ is approximately satisfied:

$$\begin{bmatrix} S_{11}^0 & S_{12}^0 \\ S_{12}^0 & S_{22}^0 \end{bmatrix} \begin{bmatrix} Q_{11}^0 & Q_{12}^0 \\ Q_{12}^0 & Q_{22}^0 \end{bmatrix} = \begin{bmatrix} 1 & 0 \\ 0 & 1 \end{bmatrix}, \tag{3}$$

$$q_{22} = \frac{p_{22}(Q_{22}^0)^2}{1 + p_{22}Q_{22}^0}, \quad q_{12} = -\frac{S_{12}^0}{S_{11}^0}q_{22}, \quad S_{12}^0 q_{12} \ll 1, \quad Q_{11}^0 Q_{22}^0 \gg \left(Q_{12}^0\right)^2, \tag{4}$$

$$\exp\left(-\frac{t}{T'}\right) = \frac{Q_{22}^0 \exp\left(-\dfrac{t}{T}\right)}{Q_{22}^0 - q_{22}\left\{1 - \exp\left(-\dfrac{t}{T}\right)\right\}}. \tag{5}$$

Derivation of equations (3) to (5) is described in Appendix 1. First, S_{ij}^0, p_{22}, and T' are empirically determined. Then, Q_{ij}^0, q_{22} and q_{12} are calculated by using equations (3) and (4). Finally, T is obtained by curve-fitting technique with the use of equation (5).

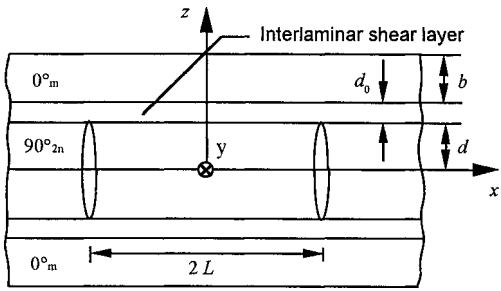

Figure 1. A shear lag model with transverse cracks [8].

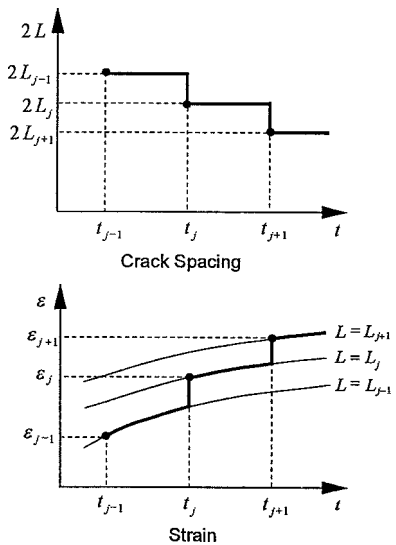

Figure 2. Change in the crack spacing and strain with time in the present model.

Figure 2 shows a schematic drawing of crack spacing and strain as a function of time. The crack spacing is constant $(2L_j)$ during time $t_j \leqslant t < t_{j+1}$. The strain response to uniaxial stress $\sigma_x(t)$ at $t_k \leqslant t < t_{k+1}$ is obtained as

$$\boldsymbol{\varepsilon}(t) = \begin{Bmatrix} \varepsilon_x(t) \\ \varepsilon_y(t) \end{Bmatrix} = \boldsymbol{\varepsilon}^0(t) + \boldsymbol{K}(t)\frac{\tanh(L_k\alpha)}{L_k\alpha}, \tag{6}$$

where $\boldsymbol{\varepsilon}^0(t)$ denotes the strain response of an intact laminate, α denotes the shear lag parameter and $\boldsymbol{K}(t)$ is a vector. The detail is given in Appendix 2. Assuming a continuous function of the transverse crack density, the longitudinal strain at an arbitrary time is written as

$$\varepsilon_x(t, \sigma_x) = \varepsilon_x^0(t) + K_x(t)\frac{2\rho(t, \sigma_x)}{\alpha}\tanh\frac{\alpha}{2\rho(t, \sigma_x)}, \tag{7}$$

with

$$K_x(t) = \frac{d}{b}\frac{\sigma_{x0}^{(2)}(t)}{Q_{11}^0}, \tag{8}$$

where $\varepsilon_x^0(t)$ is the x component of $\boldsymbol{\varepsilon}^0(t)$, $\rho(t, \sigma_x)$ is the crack density which is the inverse of $2L(t, \sigma_x)$, b and d are thickness of the 0° and 90° ply, respectively, and $\sigma_{x0}^{(2)}(t)$ is the uniform stress of the 90° ply composed of the mechanical and thermal stresses.

Using equations (1) and (2) together with some approximations (see Appendix 3), $\boldsymbol{\varepsilon}^0(t)$ and $\sigma_{x0}^{(2)}(t)$ are given by equations (A3.10) and (A3.12) for constant loading and by (A3.14) and (A3.15) for linear loading, respectively.

2.2. Transverse crack density

2.2.1. Reliability probability function. Based on the probabilistic theory associated with transverse cracking [7–9, 11], it is assumed that a 90°-ply is divided into unit elements with a volume of V (length $2L$). Here we apply the time-dependent Weibull distribution [12, 14] to transverse cracking. The reliability probability function of each unit element in the 90° ply is expressed as a function of time t and the 90° ply stress $\sigma_x^{(2)}$ by

$$R(t, \sigma_x^{(2)}) = \exp\left\{ -\int_V \Psi\left[\int_0^t \phi\left[\sigma_x^{(2)}\right] \mathrm{d}t \right] \mathrm{d}V \right\}. \tag{9}$$

A two-parameter Weibull function and the power law break-down rule are assumed:

$$\Psi(\xi) = A\xi^p, \quad \phi(\eta) = B\eta^q, \tag{10}$$

where A and p are the Weibull shape and scale parameters, respectively, and B and q are constants. Using $\sigma_x^{(2)}(x, t) = g(x)\sigma_x(t)$, where $\sigma_x(t)$ and $g(x)$ are the laminate stress and a function of x, respectively, substitution of equation (10) into equation (9) gives

$$R(t, \sigma_x) = \exp\left\{ -V_E A\left[B \int_0^t \left\{\sigma_x(t)\right\}^q \mathrm{d}t \right]^p \right\}, \tag{11}$$

with

$$V_E = \frac{V}{L}\int_0^L \{g(x)\}^{pq}\,\mathrm{d}x, \tag{12}$$

where V_E is called as the effective volume which is related to the stress distribution and size effects. The transverse crack density is assumed to be expressed as

$$\rho(t, \sigma_x) = \{1 - R(t, \sigma_x)\}\rho_s, \tag{13}$$

where ρ_s is the saturation crack density which is assumed to be independent of stress rate.

2.2.2. Monotonic and bilinear loading. The laminate stress for monotonic loading (Fig. 3a) is expressed as

$$\sigma_x(t) = \dot{\sigma}_x t, \quad (0 < t), \tag{14}$$

where $\dot{\sigma}_x$ is the stress rate. Substituting equation (14) into equation (11) gives the reliability probability function as

$$R_1(\sigma_x(t)) = \exp\left(-b\dot{\sigma}_x^{-n}\sigma_x(t)^{m+n}\right), \tag{15}$$

with

$$m = pq, \quad n = p, \quad b = \left(\frac{n}{m+n}\right)^n AB^n V_E, \tag{16}$$

where b, m and n are empirically determined constants.

Next we consider the bilinear test where the stress rate changes at a stress of σ^* (Fig 3b). The stress is given as follows:

$$\sigma_x(t) = \begin{cases} \dot{\sigma}_1 t & (0 < t < \sigma^*/\dot{\sigma}_1) \\ \dot{\sigma}_2 t + \sigma^*(1 - \dot{\sigma}_2/\dot{\sigma}_1) & (\sigma^*/\dot{\sigma}_1 \leqslant t), \end{cases} \tag{17}$$

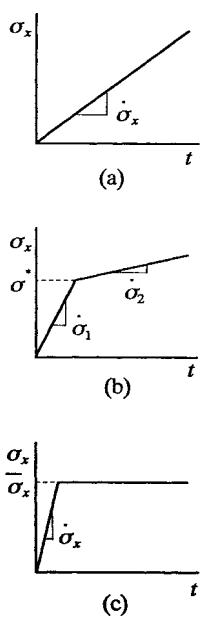

Figure 3. Schematic of three types of loading conditions; (a) monotonic loading, (b) bilinear loading and (c) constant loading.

where $\dot{\sigma}_1$ and $\dot{\sigma}_2$ are the primary and secondary stress rate, respectively. The reliability probability function for the bilinear test is obtained as

$$R_2(\sigma_x(t)) = \begin{cases} \exp\left(-b\dot{\sigma}_1^{-n}\sigma_x(t)^{m+n}\right) & (0 < t < \sigma^*/\dot{\sigma}_1) \\ \exp\left[-b\left\{\sigma_x(t)^{\frac{m+n}{n}}/\dot{\sigma}_2 + \sigma^{*\frac{m+n}{n}}(1/\dot{\sigma}_1 - 1/\dot{\sigma}_2)\right\}^n\right] & (\sigma^*/\dot{\sigma}_1 \leqslant t). \end{cases} \tag{18}$$

2.2.3. Constant loading. The laminate stress for constant loading (Fig. 3c) is written as

$$\sigma_x(t) = \begin{cases} \dot{\sigma}_x t & (0 < t < \bar{\sigma}_x/\dot{\sigma}_x) \\ \bar{\sigma}_x & (\bar{\sigma}_x/\dot{\sigma}_x \leqslant t), \end{cases} \tag{19}$$

where $\bar{\sigma}_x$ is the constant stress. The reliability probability function is calculated as

$$R_3(t, \bar{\sigma}_x) = \lim_{\dot{\sigma}_2 \to 0} R_2 = \exp\left[-b\bar{\sigma}_x^m\left(\frac{m+n}{n}t - \frac{m}{n}\frac{\bar{\sigma}_x}{\dot{\sigma}_x}\right)^n\right] \quad (\bar{\sigma}_x/\dot{\sigma}_x \leqslant t). \tag{20}$$

Another expression for the transverse crack density under constant loading is given by [17]

$$\rho(t, \bar{\sigma}_x) = \left[1 - R_4(t, \bar{\sigma}_x)\right]\left\{\rho_s - \rho_0(\bar{\sigma}_x)\right\} + \rho_0(\bar{\sigma}_x) \quad (0 < t), \tag{21}$$

where

$$R_4(t, \bar{\sigma}_x) = \lim_{\dot{\sigma}_x \to \infty} R_3(t, \bar{\sigma}_x) = \exp\left[-b\bar{\sigma}_x^m\left(\frac{m+n}{n}t\right)^n\right], \tag{22}$$

$$\rho_0(\bar{\sigma}_x) = \left\{1 - R_1(\bar{\sigma}_x)\right\}\rho_s. \tag{23}$$

Substitution of equations (22) and (23) into equations (21) leads to

$$\rho(t, \bar{\sigma}_x) = \left[1 - R_1(\bar{\sigma}_x)R_4(t, \bar{\sigma}_x)\right]\rho_s. \tag{24}$$

It should be noted that $R_1(\bar{\sigma}_x)R_4(t, \bar{\sigma}_x)$ is identical to $R_3(t, \bar{\sigma}_x)$ when time approaches to infinity.

2.2.4. Determination and meaning of the parameters. From equations (13) and (15), we obtain

$$Y = (m+n)X + \ln b, \tag{25}$$

with

$$X = \ln \sigma_x, \quad Y = \ln\left\{\ln\left(\frac{\rho_S}{\rho_S - \rho}\right)\right\} + n \ln \dot{\sigma}_x. \tag{26}$$

First, the value of Y are plotted against X for the monotonic loading test at various stress rates. The value of n is determined so that the $X-Y$ plots converges on one

master line. Then, $m + n$ and $\ln b$ are obtained by least square fitting of the above plots.

The reliability probability function in the present model is related with a time-independent two-parameter Weibull function. When n approaches zero while m is kept constant, equations (15) and (20) yield a time-independent function as

$$R_1 = R_3 = \exp\left(-b\sigma_x^m\right). \tag{27}$$

This is the same expression as a two-parameter Weibull function expressed by

$$R = \exp\left[-\left(\frac{\sigma_x}{\sigma_0}\right)^r\right], \tag{28}$$

where r and σ_0 are the scatter parameter and the characteristic strength for linear loading, respectively. Comparing equation (28) with equation (15), we obtain

$$r = m + n, \quad \sigma_0 = \left(\frac{\dot{\sigma}_x^n}{b}\right)^{1/r}. \tag{29}$$

3. EXPERIMENTAL

Specimens with a width of 8 mm were cut out of CF/Epoxy laminates with T800H/#3631 (Toray prepreg). Two strain gauges with a gauge length of 30 mm were adhesively bonded to the specimens at a temperature of 110°C for two hours to avoid hardening of the adhesive layer during the tests. The monotonic tensile, bilinear tensile and constant load tests were conducted at a temperature of 110°C to measure the strain and transverse crack density as a function of time. The stress rates $\dot{\sigma}_x$, combinations of the stress rates $(\dot{\sigma}_1, \dot{\sigma}_2)$ and the stresses σ^* and $\bar{\sigma}_x$ are listed in Table 1. The number of specimens used for each $\dot{\sigma}_x$ in the monotonic tensile tests and for each $(\dot{\sigma}_1, \dot{\sigma}_2)$ in the bilinear tensile tests are five and two, respectively. The constant load tests are conducted at $\bar{\sigma}_x$ 510 and 530 MPa, making use of three specimens per stress level.

Table 1.
Stress rates and stresses in the monotonic tensile, bilinear tensile and constant load tests

Loading type	$\dot{\sigma}_x$ or $(\dot{\sigma}_1, \dot{\sigma}_2)$ (MPa/s)	$\bar{\sigma}_x$ or σ^* (MPa)
Monotonic	0.8, 0.08,	—
	0.008, 0.0016	—
Bilinear	(0.08, 0.0016)	480
	(0.0016, 0.08)	480
Creep	4.25	510
	4.42	530

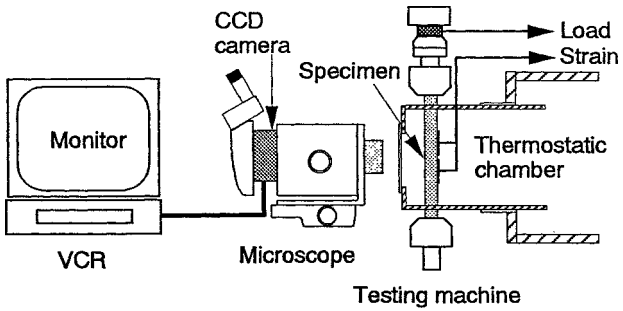

Figure 4. Experimental set-up for *in-situ* observation of transverse cracking during loading at a high temperature.

Table 2.
The shear lag parameter and material properties in equations (1) and (2) [17]

S_{11}^0 (GPa^{-1})	6.58×10^{-3}	S_{12}^0 (GPa^{-1})	-2.35×10^{-3}	S_{22}^0 (GPa^{-1})	0.153
Q_{11}^0 (GPa)	153	Q_{12}^0 (GPa)	2.34	Q_{22}^0 (GPa)	6.56
p_{22} (GPa^{-1})	0.0139	q_{12} (GPa)	0.195	q_{22} (GPa)	0.546
T' (s)	421	T (s)	419	α (cm^{-1})	33.9

Figure 4 shows the experimental setup for the tests. An electrohydraulic testing machine (MTS system 320.04) was used together with a thermostatic chamber. Transverse cracking was monitored *in-situ* by a stereoscopic microscope and recorded by a VCR through a CCD camera. Transverse crack density was measured within the range of 60 mm length corresponding to the total gauge length of the two strain gauges. The time at which transverse cracking took place was recognized with the use of both the measured strain data and *in-situ* observation.

The parameters b, m and n were determined from the results of the monotonic tensile tests at four different stress rates using equation (25). The shear lag parameter α was calculated from the strain increment due to transverse cracking during the constant load tests, and the creep compliance and relaxation modulus expressed by equations (1) and (2), respectively, were determined from the results of tensile tests and creep tests of [0°] and [90°] specimens [17]. These constants are summarized in Table 2.

4. RESULTS AND DISCUSSION

4.1. Monotonic tensile tests

Figure 5 shows the effect of stress rate on the change in the transverse crack density. The crack density at lower rates is larger than that at higher rates. The specimens for $\dot{\sigma}_x$ 0.8, 0.08 and 0.008 MPa/s were broken before the transverse crack density reached the saturation value (7/cm). This is partly because the delamination takes

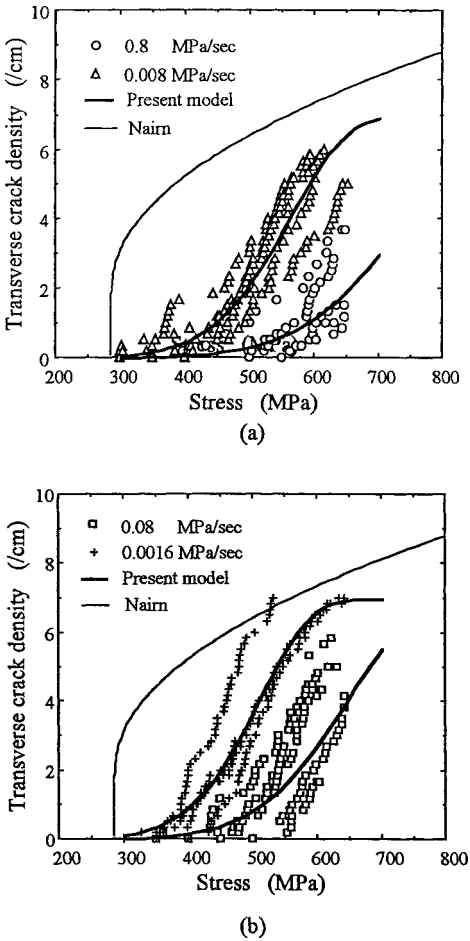

Figure 5. Effects of stress rates on change in the transverse crack density in the monotonic tensile tests; (a) 0.8 and 0.008 MPa/s and (b) 0.08 and 0.0016 MPa/s. The solid lines are obtained by using the present model and Nairn's model [18].

place at a high stress and partly because the final failure occurs under the end tab. Averaged first ply failure (FPF) and final failure (FF) stresses are presented in Table 3. FPF stresses at lower stress rates are smaller than those at higher rates. There are two reasons for this rate-dependence. First, since a low stress rate leads to high compliance of 90°-ply, the stress required for cracking decreases if the transverse cracking occurs at a critical failure strain. Secondly, there is much time for delayed fracture to occur at lower rates before the stress or strain reaches a critical one. On the other hand, FF stress is insensitive to stress rate because the strength of the cross-ply laminate largely depends on those of the 0°-ply.

Figure 6 shows typical stress–strain curves for four stress rates. The strains are averaged out of the two strain gages data with a total gage length of 60 mm. The slopes of curves for a stress rate $\dot{\sigma}_x$ of 0.08, 0.008 and 0.0016 MPa/s gradually

Table 3.
FPF and FF stresses in monotonic tensile tests at various stress rates

Stress rate (MPa/s)	0.8	0.08	0.008	0.0016
FPF stress (MPa)	484	461	350	348
FF stress (MPa)	639	622	611	619

Table 4.
The parameters for expressing the transverse crack density

ρ_s (/cm)	7.0	m	6.98
b ($GPa^{-m}s^{-n}$)	0.317	n	0.450

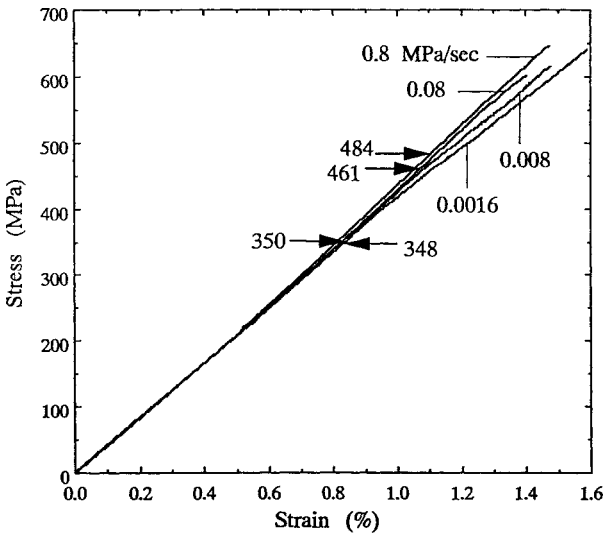

Figure 6. Typical stress–strain curves for four different stress rates in the monotonic tensile tests; Arrows show the averaged FPF stress for each stress rate.

decrease with increasing transverse crack density. Before transverse cracking occurs, the difference due to the different stress rates is not remarkable because the viscoelastic effect of the 90°-ply on overall strain is relatively small.

With the aid of the data in Fig. 5, X and Y in equation (26) are determined and plotted in Fig. 7. The parameters obtained with these plots are presented in Table 4. The transverse crack densities in the monotonic tensile tests on the basis of equation (13) and the above parameters are depicted as bold solid lines in Fig. 5. For comparison, the crack density predicted using by Nairn's variational approach [18] is also depicted. The crack density increases rapidly at a critical strength in his model while it increases gently in the present statistical model which gives better agreement with experimental results. A statistical approach can explain cracking behaviour phenomenologically, however, it provides less physical understanding than a fracture mechanical approach. An energy-based model including the viscoelastic effect should be established in the future work.

4.2. Bilinear tensile tests

Figure 8 shows the measured and predicted transverse crack density as a function of the stress in the bilinear tensile tests. The bold solid lines denote predictions for the bilinear tensile tests. A sudden increase in the crack density is observed when the stress rate changes from high to low; on the other hand, the crack density gradually

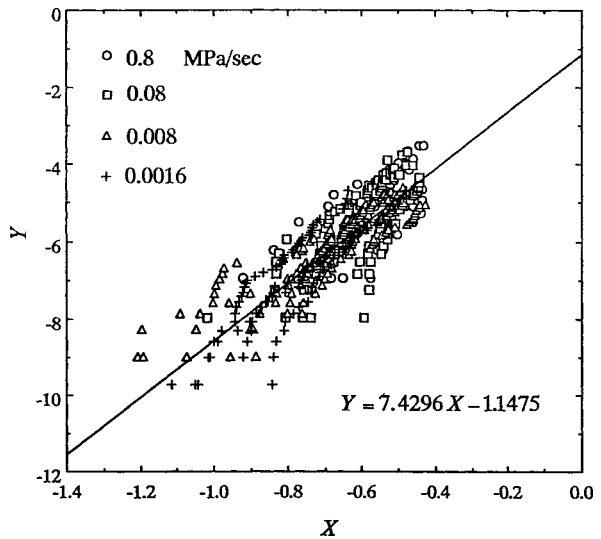

Figure 7. The $X-Y$ plots in equation (25) for four different stress rates in the monotonic tensile tests; the solid line is obtained by least square fitting.

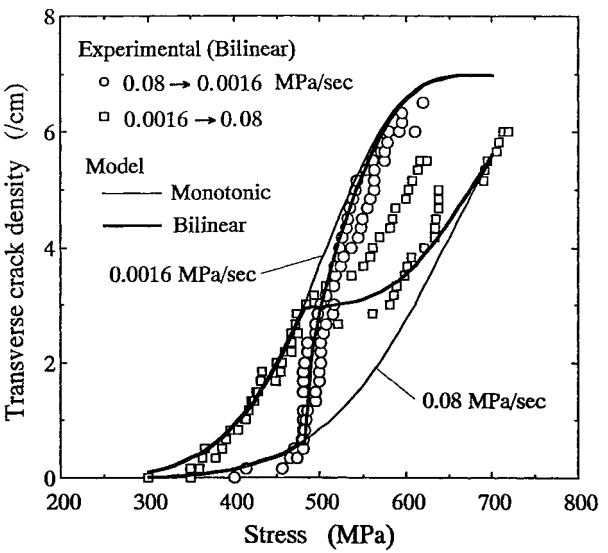

Figure 8. Measured and predicted transverse crack density against stress during the bilinear tensile tests for two combinations of the stress rates.

approaches to the one of the high rate when the stress rate changes from low to high. These phenomena are well predicted using the present model. Figures 9a and b show the comparison of stress–strain curves between the experimental results and theoretical predictions for $(\dot{\sigma}_1, \dot{\sigma}_2) = (0.08, 0.0016)$ and $(\dot{\sigma}_1, \dot{\sigma}_2) = (0.0016, 0.08)$ MPa/s, respectively. Measured and predicted tangent Young's moduli in Fig. 9a are reduced from 43.4 and 41.8 (for $300 < \sigma_x < 480$) to 36.7 and 37.1 GPa (for $480 < \sigma_x$), respectively. Difference in the Young's modulus for $300 < \sigma_x < 480$ is mainly caused by the inverse nonlinearity of 0°-ply in the longitudinal direction

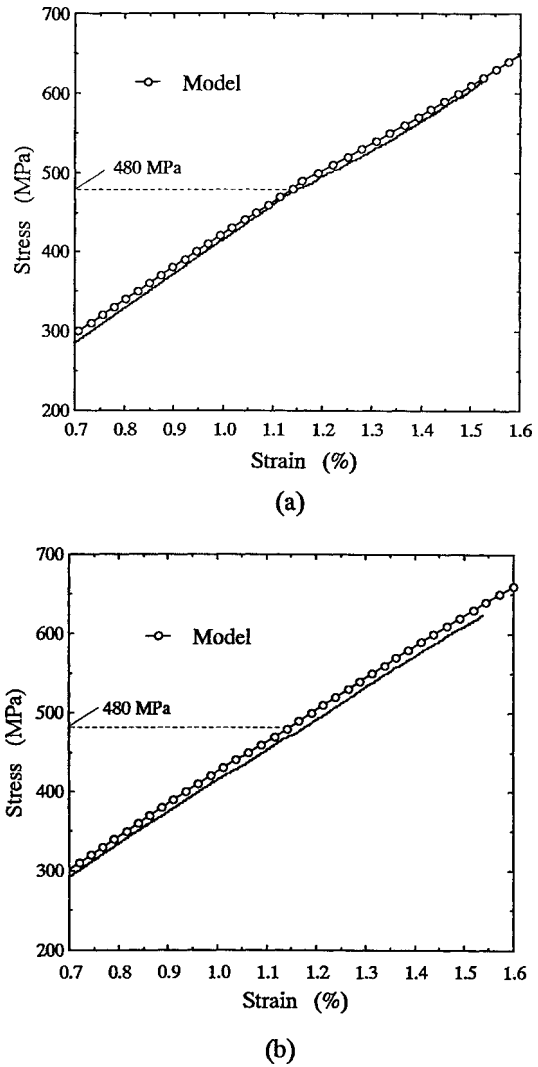

Figure 9. Measured and predicted stress–strain curves during the bilinear tensile tests; (a) $(\dot{\sigma}_1, \dot{\sigma}_2) = (0.08, 0.0016)$ MPa/s and (b) $(\dot{\sigma}_1, \dot{\sigma}_2) = (0.0016, 0.08)$ MPa/s.

which leads to a concave stress–strain curve. Lower measured modulus for $480 < \sigma_x$ may be due to local delamination from transverse crack tips.

4.3. Constant load tests

Figure 10 shows the strain during a constant load test at 510 MPa [17]. Abrupt increases in the strain are the results of transverse cracking. The strains predicted

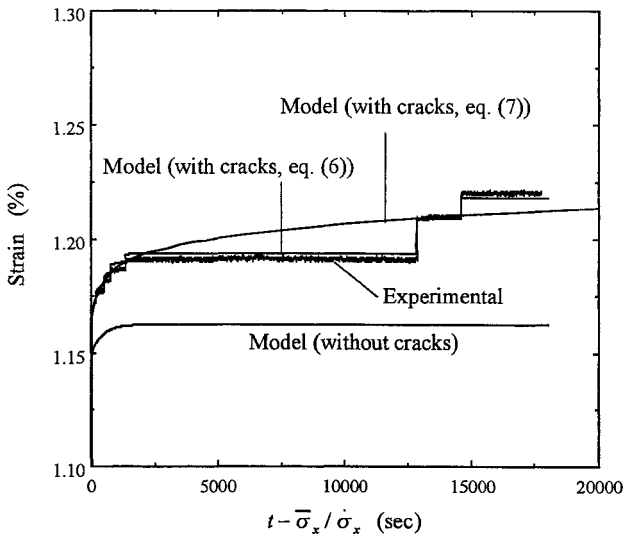

Figure 10. Measured and predicted (equations (6) and (7)) strains during a constant load test of a $[0/90_3^\circ]_S$ specimen at a stress of 510 MPa [17].

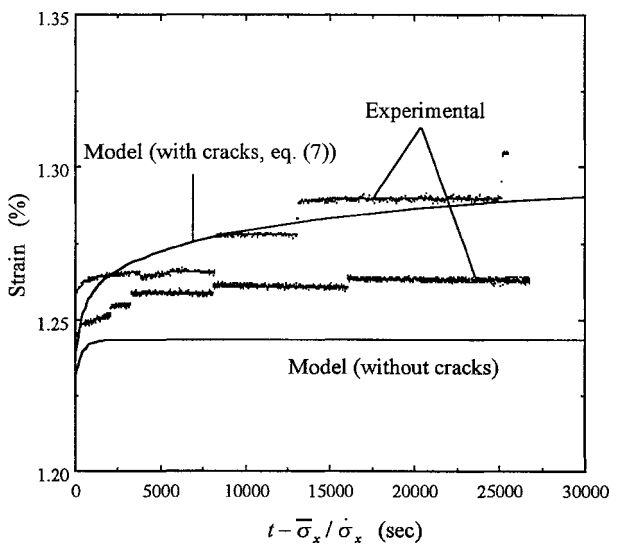

Figure 11. Comparison of the strains during a constant load tests at 530 MPa between the experimental results and predictions (equation (7)).

using equations (6) and (7) are also shown in this figure. Equation (6) gives better agreement with the experimental results because the measured crack density is employed. Figure 11 shows a comparison of the strain during the constant load tests between the experimental and predicted (equation (7)) results. The predicted strain bases on a continuous increase in the crack density while the measured strain increases discontinuously. However, the final strain increase for the same number of cracks is comparable and thus the validity of the present model is verified with the above results.

5. CONCLUSIONS

A model is developed to predict the transverse crack density and strain response in a cross-ply laminate under monotonic, bilinear and constant loading using viscoelasticity, shear lag analysis and a probabilistic failure model. The crack density and strain response under both bilinear and constant loading are predicted based on the model using the parameters determined with the aid of the results of monotonic tensile tests. It is shown that the model provides good agreement with the experimental results.

Acknowledgements

The present research was supported in part by grant-in-aid (No. 09751009) for Scientific Research of the Ministry of Education, Science, Sports and Culture of Japan.

REFERENCES

1. Y. C. Lou and R. A. Shapery, Viscoelastic characterization of a nonlinear fiber-reinforced plastic, *J. Compos. Mater.* **5**, 208–234 (1971).
2. A. Horoschenkoff, Characterization of the creep compliances J_{22} and J_{66} of orthotropic composites with PEEK and epoxy matrices using the nonlinear viscoelastic response of the neat resins, *J. Compos. Mater.* **24**, 879–891 (1990).
3. D. A. Dillard, D. H. Morris and H. F. Brinson, Predicting viscoelastic response and delayed failures in general laminated composites, in: *Composite Materials: Testing and Design* (Sixth Conference), *ASTM STP 787*, I. M. Daniel (Ed.), pp. 357–370. American Society of Testing and Materials, Philadelphia (1982).
4. D. A. Dillard and H. F. Brinson, A numerical for predicting creep and delayed failures in laminated composites, in: *Long-term Behavior of Composites, ASTM STP 813*, T. K. O'Brien (Ed.), pp. 23–37. American Society of Testing and Materials, Philadelphia (1983).
5. D. L. Flaggs and F. W. Crossman, Analysis of the viscoelastic response of composite laminates during hygrothermal exposure, *J. Compos. Mater.* **15**, 21–40 (1981).
6. I. Chung, C. T. Sun and I. Y. Chang, Modeling creep in thermoplastic composites, *J. Compos. Mater.* **27**, 1009–1029 (1993).
7. P. W. Manders, T. W. Chou, F. R. Jones and J. W. Rock, Statistical analysis of multiple fracture in $0^\circ/90^\circ/0^\circ$ glass fibre/epoxy resin laminates, *J. Mater. Sci.* **18**, 2876–2889 (1983).

8. H. Fukunaga, T. W. Chou, P. W. M. Peters and K. Schulte, Probabilistic failure strength analysis of graphite/epoxy cross-ply laminates, *J. Compos. Mater.* **18**, 339–356 (1984).
9. P. W. M. Peters, The strength distribution of 90° plies in 0/90/0 graphite-epoxy laminates, *J. Compos. Mater.* **18**, 545–556 (1984).
10. G. Lim and C. S. Hong, Prediction of transverse cracking and stiffness reduction in cross-ply laminated composites, *J. Compos. Mater.* **23**, 695–713 (1989).
11. N. Takeda and S. Ogihara, *In-situ* observation and probabilistic prediction of microscopic failure processes in CFRP cross-ply laminates, *Compos. Sci. Technol.* **52**, 183–195 (1994).
12. B. D. Coleman, Statistics and time dependence of mechanical breakdown in fibers, *J. Applied Phys.* **29**, 968–983 (1958).
13. S. L. Phoenix, P. Schwarts and H. H. Robinson, IV, Statistics for the strength and lifetime in creep-rupture of model carbon/epoxy composites, *Compos. Sci. Technol.* **32**, 81–120 (1998).
14. K. Goda and J. Hamada, Creep-rupture lifetime distribution of boron fibers, *Mater. Sci. Res. International* **2**, 123–130 (1996).
15. R. H. Moore and D. A. Dillard, Time-dependent matrix cracking in cross-ply laminates, *Compos. Sci. Technol.* **39**, 1–12 (1990).
16. J. Raghavan and M. Meshii, Time-dependent damage in carbon fibre-reinforced polymer composites, *Composites* **27A**, 1223–1227 (1996).
17. K. Ogi and Y. Takao, Modeling a creep behavior of cross-ply laminates with progressive transverse cracking, *Advanced Compos. Mater.* **8**, 189–203 (1999).
18. J. A. Nairn, The strain energy release rate of composite microcracking: a variational approach, *J. Compos. Mater.* **23**, 1106–1129 (1989).

APPENDIX 1. DERIVATION OF EQUATIONS (3), (4) AND (5)

Let a matrix $\boldsymbol{A}(t)$ equal $\boldsymbol{S}(t)\boldsymbol{Q}(t)$ given by equations (1) and (2), the components of $\boldsymbol{A}(t)$ are written as

$$
\begin{aligned}
A_{11}(t) &= \left(S_{11}^0 Q_{11}^0 + S_{12}^0 Q_{12}^0\right) - S_{12}^0 q_{12}\left(1 - \exp\left(-\frac{t}{T}\right)\right),\\
A_{12}(t) &= \left(S_{11}^0 Q_{12}^0 + S_{12}^0 Q_{22}^0\right) - \left(S_{11}^0 q_{12} + S_{12}^0 q_{22}\right)\left(1 - \exp\left(-\frac{t}{T}\right)\right),\\
A_{21}(t) &= \left(S_{12}^0 Q_{11}^0 + S_{22}^0 Q_{12}^0\right) - S_{22}^0 q_{12}\left(1 - \exp\left(-\frac{t}{T}\right)\right)\\
&\quad + p_{22} Q_{12}^0\left(1 - \exp\left(-\frac{t}{T'}\right)\right)\\
&\quad - p_{22} q_{12}\left(1 - \exp\left(-\frac{t}{T}\right)\right)\left(1 - \exp\left(-\frac{t}{T'}\right)\right),\\
A_{22}(t) &= \left(S_{12}^0 Q_{12}^0 + S_{22}^0 Q_{22}^0\right) - S_{12}^0 q_{12}\left(1 - \exp\left(-\frac{t}{T}\right)\right)\\
&\quad - S_{22}^0 q_{22}\left(1 - \exp\left(-\frac{t}{T}\right)\right)\\
&\quad + p_{22} Q_{22}^0\left(1 - \exp\left(-\frac{t}{T'}\right)\right)\\
&\quad - p_{22} q_{22}\left(1 - \exp\left(-\frac{t}{T}\right)\right)\left(1 - \exp\left(-\frac{t}{T'}\right)\right). \qquad \text{(A1.1)}
\end{aligned}
$$

From $\boldsymbol{A}(0) = \boldsymbol{I}$, we have

$$\begin{bmatrix} S_{11}^0 & S_{12}^0 \\ S_{12}^0 & S_{22}^0 \end{bmatrix} \begin{bmatrix} Q_{11}^0 & Q_{12}^0 \\ Q_{12}^0 & Q_{22}^0 \end{bmatrix} = \begin{bmatrix} 1 & 0 \\ 0 & 1 \end{bmatrix}. \tag{A1.2}$$

Next, the following relations are necessary for $\lim_{t\to\infty} \boldsymbol{A}(t) = \boldsymbol{I}$

$$S_{12}^0 q_{12} = 0, \tag{A1.3.1}$$

$$S_{11}^0 q_{12} + S_{12}^0 q_{22} = 0, \tag{A1.3.2}$$

$$-S_{22}^0 q_{12} + p_{22} Q_{12}^0 - p_{22} q_{12} = 0, \tag{A1.3.3}$$

$$-S_{12}^0 q_{12} - S_{22}^0 q_{22} + p_{22} Q_{22}^0 - p_{22} q_{22} = 0. \tag{A1.3.4}$$

Because $S_{12}^0 q_{12}$ is sufficiently small compared with unity, equation (A1.3.1) approximately holds good. Combination of equations (A1.2), (A1.3.2) and (A1.3.4) gives

$$q_{12} = \frac{p_{22} Q_{12}^0 Q_{22}^0}{1 + p_{22} Q_{22}^0}, \quad q_{22} = \frac{p_{22} \left(Q_{22}^0\right)^2}{1 + p_{22} Q_{22}^0}. \tag{A1.4}$$

Using equations (A1.2) and (A1.4), the left hand of equation (A1.3.3) yields

$$-S_{22}^0 q_{12} + p_{22} Q_{12}^0 - p_{22} q_{12} = -\frac{p_{22} Q_{12}^0}{1 + p_{22} Q_{22}^0} \frac{\left(Q_{12}^0\right)^2}{Q_{11}^0 Q_{22}^0 - \left(Q_{12}^0\right)^2}. \tag{A1.5}$$

This term is negligible because of $(Q_{12}^0)^2 \ll Q_{11}^0 Q_{22}^0$. Using the above equations, equation (A1.1) leads to

$$\begin{aligned} A_{11}(t) &= 1, \\ A_{12}(t) &= 0, \\ A_{21}(t) &= p_{22} Q_{12}^0 \exp\left(-\frac{t}{T}\right) - \frac{p_{22} Q_{12}^0}{1 + p_{22} Q_{22}^0} \exp\left(-\frac{t}{T'}\right) \\ &\quad - \frac{p_{22}^2 Q_{12}^0 Q_{22}^0}{1 + p_{22} Q_{22}^0} \exp\left(-\frac{t}{T}\right) \exp\left(-\frac{t}{T'}\right), \\ A_{22}(t) &= 1 - \frac{Q_{22}^0}{Q_{12}^0} A_{21}(t). \end{aligned} \tag{A1.6}$$

Thus, the following relation between the two time constants T and T' is needed for $\boldsymbol{A}(t) = \boldsymbol{I}$ at any time t:

$$\exp\left(-\frac{t}{T}\right) = \frac{\exp\left(-\dfrac{t}{T'}\right)}{1 + p_{22}Q_{22}^{0}\left\{1 - \exp\left(-\dfrac{t}{T'}\right)\right\}}. \tag{A1.7}$$

APPENDIX 2. STRAIN RESPONSE BASED ON A SHEAR LAG ANALYSIS

At first, strain response under the constant crack density is obtained based on a shear lag model shown in Fig. 1. The displacements in the x and y directions, denoted by u and v, are assumed to be uniform through the thickness in each ply and decomposed into the linear component and the component expressed as a function of x and t as

$$u^{(k)}(x,t) = \varepsilon_x^0(t)x + U^{(k)}(x,t), \quad v^{(k)}(x,y,t) = \varepsilon_y^0(t)y + V^{(k)}(x,t) \quad (k = 1, 2), \tag{A2.1}$$

where the superscripts 1 and 2 represent the 0° and 90° plies, respectively, $\varepsilon_x^0(t)$ and $\varepsilon_y^0(t)$ are the strains of an intact laminate under the applied stress $\sigma_x(t)$, and $U^{(k)}$ and $V^{(k)}$ are functions of x and t. Next, it is assumed that the interlaminar shear layer with the thickness d_0 and the shear modulus $G(t)$ undergoes the shear stresses $\tau_{xz}(x,t)$ and $\tau_{yz}(x,t)$ given by the following hereditary integrals:

$$\begin{aligned} \tau_{xz}(x,t) &= G(t)\gamma_{xz}(x,0) + \int_0^t G(t-\tau)\frac{\partial \gamma_{xz}(x,\tau)}{\partial \tau}\,\mathrm{d}\tau, \\ \tau_{yz}(x,t) &= G(t)\gamma_{yz}(x,0) + \int_0^t G(t-\tau)\frac{\partial \gamma_{yz}(x,\tau)}{\partial \tau}\,\mathrm{d}\tau, \end{aligned} \tag{A2.2}$$

where $\gamma_{xz}(x,t)$ and $\gamma_{yz}(x,t)$ denote the engineering shear strains which are assumed to be proportional to the difference in the displacements across the interlaminar shear layer. The strains in each ply and the interlaminar shear layer are obtained form equation (A2.1) as

$$\begin{aligned} \varepsilon_x^{(k)}(x,t) &= \varepsilon_x^0(t) + \varepsilon_x^{(k)^T} + \frac{\partial U^{(k)}(x,t)}{\partial x}, \\ \varepsilon_y^{(k)}(t) &= \varepsilon_y^0(t) + \varepsilon_y^{(k)^T}, \\ \gamma_{xy}^{(k)}(x,t) &= \frac{\partial V^{(k)}(x,t)}{\partial x}, \end{aligned} \tag{A2.3}$$

where $\varepsilon_x^{(k)^T}$ and $\varepsilon_y^{(k)^T}$ denote the thermal strains with respect to x and y directions in the k-th ply, respectively, and

$$\gamma_{xz}(x,t) = \frac{U^{(1)}(x,t) - U^{(2)}(x,t)}{d_0},$$
$$\gamma_{yz}(x,t) = \frac{V^{(1)}(x,t) - V^{(2)}(x,t)}{d_0}. \tag{A2.4}$$

The viscoelastic constitutive equation in each ply is given by

$$\sigma^{(k)}(x,t) = \boldsymbol{Q}^{(k)}(t)\boldsymbol{\varepsilon}^{(k)}(x,0) + \int_0^t \boldsymbol{Q}^{(k)}(t-\tau)\frac{\partial \boldsymbol{\varepsilon}^{(k)}(x,\tau)}{\partial \tau}\,\mathrm{d}\tau, \tag{A2.5}$$

where $\sigma^{(k)}(x,t)$, $\boldsymbol{\varepsilon}^{(k)}(x,t)$ and $\boldsymbol{Q}^{(k)}(t)$ refer respectively to the stress vector, strain vector and stiffness matrix in each ply expressed as

$$\sigma^{(k)}(x,t) = \begin{Bmatrix} \sigma_x^{(k)}(x,t) \\ \sigma_y^{(k)}(x,t) \\ \tau_{xy}^{(k)}(x,t) \end{Bmatrix}, \quad \boldsymbol{\varepsilon}^{(k)}(x,t) = \begin{Bmatrix} \varepsilon_x^{(k)}(x,t) \\ \varepsilon_y^{(k)}(x,t) \\ \gamma_{xy}^{(k)}(x,t) \end{Bmatrix},$$
$$\boldsymbol{Q}^{(k)}(t) = \begin{bmatrix} Q_{11}^{(k)}(t) & Q_{12}^{(k)}(t) & 0 \\ Q_{12}^{(k)}(t) & Q_{22}^{(k)}(t) & 0 \\ 0 & 0 & Q_{66}^{(k)}(t) \end{bmatrix}. \tag{A2.6}$$

The equilibrium equations in each ply are given by

$$b\frac{\partial \sigma_x^{(1)}}{\partial x} - \tau_{xz} = 0, \quad d\frac{\partial \sigma_x^{(2)}}{\partial x} + \tau_{xz} = 0, \tag{A2.7.1}$$

$$b\frac{\partial \tau_{xy}^{(1)}}{\partial x} - \tau_{yz} = 0, \quad d\frac{\partial \tau_{xy}^{(2)}}{\partial x} + \tau_{yz} = 0, \tag{A2.7.2}$$

where b and d denote the thickness of the 0° ply and 90° ply. Taking Laplace transforms of equations (A2.2), (A2.3), (A2.4), (A2.5), and (A2.7), we find the constitutive equations, strains in each ply and equilibrium equations in the transformed world as

$$\hat{\sigma}^{(k)}(x,s) = s\hat{\boldsymbol{Q}}^{(k)}(s)\hat{\boldsymbol{\varepsilon}}^{(k)}(x,s), \tag{A2.8}$$

$$\hat{\tau}_{xz}(x,s) = s\hat{G}(s)\frac{\hat{U}^{(1)}(x,s) - \hat{U}^{(2)}(x,s)}{d_0},$$
$$\hat{\tau}_{yz}(x,s) = s\hat{G}(s)\frac{\hat{V}^{(1)}(x,s) - \hat{V}^{(2)}(x,s)}{d_0}, \tag{A2.9}$$

$$\hat{\varepsilon}_x^{(k)}(x,s) = \hat{\varepsilon}_x^0(s) + \frac{\varepsilon_x^{(k)^T}}{s} + \frac{\partial \hat{U}^{(k)}(x,s)}{\partial x},$$
$$\hat{\varepsilon}_y^{(k)}(s) = \hat{\varepsilon}_y^0(s) + \frac{\varepsilon_y^{(k)^T}}{s}, \tag{A2.10}$$
$$\hat{\gamma}_{xy}^{(k)}(x,s) = \frac{\partial \hat{V}^{(k)}(x,s)}{\partial x},$$

$$b\frac{\partial \hat{\sigma}_x^{(1)}(x,s)}{\partial x} - \hat{\tau}_{xz}(x,s) = 0, \quad d\frac{\partial \hat{\sigma}_x^{(2)}(x,s)}{\partial x} + \hat{\tau}_{xz}(x,s) = 0, \tag{A2.11.1}$$

$$b\frac{\partial \hat{\tau}_{xy}^{(1)}(x,s)}{\partial x} - \hat{\tau}_{yz}(x,s) = 0, \quad d\frac{\partial \hat{\tau}_{xy}^{(2)}(x,s)}{\partial x} + \hat{\tau}_{yz}(x,s) = 0, \tag{A2.11.2}$$

where a circumflex accent denotes a Laplace transform. Substitution of equations (A2.8), (A2.9) and (A2.10) into equation (A2.11) leads to

$$\frac{\partial^2 \hat{U}^{(1)}}{\partial x^2} - \frac{\hat{G}}{bd_0\hat{Q}_{11}}\left(\hat{U}^{(1)} - \hat{U}^{(2)}\right) = 0, \quad \frac{\partial^2 \hat{U}^{(2)}}{\partial x^2} + \frac{\hat{G}}{dd_0\hat{Q}_{22}}\left(\hat{U}^{(1)} - \hat{U}^{(2)}\right) = 0, \tag{A2.12.1}$$

$$\frac{\partial^2 \hat{V}^{(1)}}{\partial x^2} - \frac{\hat{G}}{bd_0\hat{Q}_{66}}\left(\hat{V}^{(1)} - \hat{V}^{(2)}\right) = 0, \quad \frac{\partial^2 \hat{V}^{(2)}}{\partial x^2} + \frac{\hat{G}}{dd_0\hat{Q}_{66}}\left(\hat{V}^{(1)} - \hat{V}^{(2)}\right) = 0. \tag{A2.12.2}$$

The boundary conditions are given by

$$u^{(2)}(0,t) = 0, \quad v^{(2)}(0,0,t) = 0, \quad v^{(1)}(L,0,t) = 0,$$
$$\sigma_x^{(2)}(L,t) = 0, \quad b\sigma_x^{(1)^M}(L,t) = (b+d)\sigma_x(t), \tag{A2.13}$$

where the superscript M denotes the mechanical component. After imposing the above boundary conditions, the solutions to the differential equations (A2.12) are obtained as

$$\hat{U}^{(1)}(x,s) = \frac{d\hat{\sigma}_{x0}^{(2)}(s)}{bs\hat{\alpha}(s)\hat{Q}_{11}(s)}\frac{\sinh\{\hat{\alpha}(s)x\}}{\cosh\{\hat{\alpha}(s)L\}}, \quad \hat{V}^{(1)}(x,s) = 0,$$
$$\hat{U}^{(2)}(x,s) = -\frac{\hat{\sigma}_{x0}^{(2)}(s)}{s\hat{\alpha}(s)\hat{Q}_{22}(s)}\frac{\sinh\{\hat{\alpha}(s)x\}}{\cosh\{\hat{\alpha}(s)L\}}, \quad \hat{V}^{(2)}(x,s) = 0, \tag{A2.14}$$

with

$$\hat{\alpha}(s) = \sqrt{\frac{\hat{G}(s)}{d_0}\left(\frac{1}{b\hat{Q}_{11}(s)} + \frac{1}{d\hat{Q}_{22}(s)}\right)}, \tag{A2.15}$$

$$\hat{\sigma}_x^{(2)}(x,s) = \hat{Q}_{22}(s)\left(s\hat{\varepsilon}_x^0(s) + \varepsilon_x^{(2)^T}\right) + \hat{Q}_{12}(s)\left(s\hat{\varepsilon}_y^0(s) + \varepsilon_y^{(2)^T}\right), \tag{A2.16}$$

$$\begin{Bmatrix} \hat{\varepsilon}_x^0(s) \\ \hat{\varepsilon}_y^0(s) \end{Bmatrix} = \begin{Bmatrix} s\hat{J}_{11}(s)\hat{\sigma}_x(s) \\ s\hat{J}_{12}(s)\hat{\sigma}_x(s) \end{Bmatrix}, \tag{A2.17}$$

where $\hat{J}_{11}(s)$ and $\hat{J}_{12}(s)$ denote Laplace transforms of the creep compliance of the laminate (see Appendix 3). Hence, the strain distributions in each ply are calculated as

$$\hat{\boldsymbol{\varepsilon}}^{(1)}(x,s) = \begin{Bmatrix} \hat{\varepsilon}_x^0(s) \\ \hat{\varepsilon}_y^0(s) \\ 0 \end{Bmatrix} + \frac{1}{s}\begin{Bmatrix} \varepsilon_x^{(1)^T} \\ \varepsilon_y^{(1)^T} \\ 0 \end{Bmatrix} + \begin{Bmatrix} \dfrac{d\hat{\sigma}_{x0}^{(2)}(s)}{bs\hat{Q}_{11}(s)} \dfrac{\cosh\{\hat{\alpha}(s)x\}}{\cosh\{\hat{\alpha}(s)L\}} \\ 0 \\ 0 \end{Bmatrix}, \tag{A2.18.1}$$

$$\hat{\boldsymbol{\varepsilon}}^{(2)}(x,s) = \begin{Bmatrix} \hat{\varepsilon}_x^0(s) \\ \hat{\varepsilon}_y^0(s) \\ 0 \end{Bmatrix} + \frac{1}{s}\begin{Bmatrix} \varepsilon_x^{(2)^T} \\ \varepsilon_y^{(2)^T} \\ 0 \end{Bmatrix} + \begin{Bmatrix} -\dfrac{\hat{\sigma}_{x0}^{(2)}(s)}{s\hat{Q}_{22}(s)} \dfrac{\cosh\left\{\hat{\alpha}(s)x\right\}}{\cosh\left\{\hat{\alpha}(s)L\right\}} \\ 0 \\ 0 \end{Bmatrix}. \tag{A2.18.2}$$

The average strain in the 0° ply between the cracks is given by

$$\begin{aligned} \hat{\bar{\boldsymbol{\varepsilon}}}(s) &= \frac{1}{L}\int_0^L \hat{\boldsymbol{\varepsilon}}^{(1)}(x,s)\,\mathrm{d}x - \frac{1}{s}\begin{Bmatrix} \varepsilon_x^{(1)^T} \\ \varepsilon_y^{(1)^T} \end{Bmatrix} \\ &= \begin{Bmatrix} \hat{\varepsilon}_x^0(s) \\ \hat{\varepsilon}_y^0(s) \end{Bmatrix} + \begin{Bmatrix} \dfrac{d\hat{\sigma}_{x0}^{(2)}(s)}{bs\hat{Q}_{11}(s)} \dfrac{\tanh\left\{\hat{\alpha}(s)L\right\}}{\hat{\alpha}(s)L} \\ 0 \end{Bmatrix}. \end{aligned} \tag{A2.19}$$

The shear strain $\gamma_{xy}^{(1)}$ is omitted because it is zero. Here it is assumed that $\hat{\alpha}(s)$ is a positive constant α because the change in α is negligible when the crack density $1/2L$ changes with time under loading. The value of α can be empirically determined from the strain increment during constant loading. Then we obtain the strain response of the laminate with the crack density $1/2L$ as

$$\bar{\boldsymbol{\varepsilon}}(t) = \boldsymbol{\varepsilon}^0(t) + \boldsymbol{K}(t)\frac{\tanh\{\alpha L\}}{\alpha L} \equiv \boldsymbol{\varepsilon}(t,L) \quad (0 \leqslant t), \tag{A2.20}$$

with

$$\boldsymbol{\varepsilon}^0(t) = \begin{Bmatrix} \varepsilon_x^0(t) \\ \varepsilon_y^0(t) \end{Bmatrix}, \quad \boldsymbol{K}(t) = \begin{Bmatrix} \dfrac{d\sigma_{x0}^{(2)}(t)}{bQ_{11}^0} \\ 0 \end{Bmatrix}. \tag{A2.21}$$

Finally since the strain changes from $\varepsilon(t_{j+1}, L_j)$ to $\varepsilon(t_{j+1}, L_{j+1})$ at the moment of cracking $t = t_{j+1}$, the strain at time $t\,(t_k \leqslant t < t_{k+1})$ is given by

$$\boldsymbol{\varepsilon}(t, L_k) = \boldsymbol{\varepsilon}^0(t) + \boldsymbol{K}(t)\frac{\tanh(L_k\alpha)}{L_k\alpha} \quad (t_k \leqslant t < t_{k+1}). \tag{A2.22}$$

APPENDIX 3. CALCULATIONS OF THE STRAIN RESPONSE

Here, the strain vector $\boldsymbol{\varepsilon}^0(t)$ and the vector $\boldsymbol{K}(t)$ given by equation (A2.21) are obtained as functions of time. Laplace transform of the creep compliance of an uncracked laminate, denoted by $\hat{\boldsymbol{J}}(s)$, is given in the literature [17]. The 1-1 and 1-2 components of $\hat{\boldsymbol{J}}(s)$ for a cross-ply laminate is expressed as

$$\hat{J}_{11}(s) = (b+d)\frac{b\hat{Q}_{22}(s) + d\hat{Q}_{11}(s)}{s^2\hat{\Delta}(s)}, \tag{A3.1}$$

$$\hat{J}_{12}(s) = -\frac{(b+d)^2\hat{Q}_{12}(s)}{s^2\hat{\Delta}(s)}, \tag{A3.2}$$

with

$$\hat{\Delta}(s) = \big(b\hat{Q}_{11}(s) + d\hat{Q}_{22}(s)\big)\big(b\hat{Q}_{22}(s) + d\hat{Q}_{11}(s)\big) - \big\{(b+d)\hat{Q}_{12}(s)\big\}^2 \tag{A3.3}$$

Substituting equation (2) into equations (A3.1) and (A3.2), we obtain

$$\hat{J}_{11}(s) = (b+d)\frac{(bQ_{22}^0 + dQ_{11}^0)T^2s^2 + (2bQ_{22}^0 - bq_{22} + 2dQ_{11}^0)Ts + (bQ_{22}^0 - bq_{22} + dQ_{11}^0)}{(C_1+C_2+C_3)T^2s^3 + (2C_1+C_2)Ts^2 + C_1s}, \tag{A3.4}$$

$$\hat{J}_{12}(s) = -(b+d)^2\frac{Q_{12}^0T^2s^2 + (2Q_{12}^0 - q_{12})Ts + (Q_{12}^0 - q_{12})}{(C_1+C_2+C_3)T^2s^3 + (2C_1+C_2)Ts^2 + C_1s}, \tag{A3.5}$$

with

$$\begin{aligned} C_1 = {} & \big(b^2+d^2\big)Q_{11}^0\big(Q_{22}^0 - q_{22}\big) + bd\Big\{\big(Q_{11}^0\big)^2 + \big(Q_{22}^0 - q_{22}\big)^2\Big\} \\ & - (b+d)^2\big(Q_{12}^0 - q_{12}\big)^2, \end{aligned}$$

$$C_2 = \big\{\big(b^2+d^2\big)Q_{11}^0 + 2bd\big(Q_{22}^0 - q_{22}\big)\big\}\,q_{22} - 2(b+d)^2\big(Q_{12}^0 - q_{12}\big)q_{12}, \tag{A3.6}$$

$$C_3 = bdq_{22}^2 - (b+d)^2q_{12}^2.$$

Using $bQ_{22}^0 + dQ_{11}^0 \gg bq_{22}$, equations (A3.4) and (A3.5) are split into partial fraction as

$$\hat{J}_{11}(s) = \frac{(b+d)(bQ_{22}^0 + dQ_{11}^0)}{C_1 + C_2 + C_3}\left(\frac{B_0}{s} + \frac{B_1}{s - \phi_1/T} + \frac{B_2}{s - \phi_2/T}\right), \tag{A3.7}$$

$$\hat{J}_{12}(s) = \frac{(b+d)^2 Q_{12}^0}{C_1 + C_2 + C_3}\left(\frac{D_0}{s} + \frac{D_1}{s - \phi_1/T} + \frac{D_2}{s - \phi_2/T}\right), \tag{A3.8}$$

with

$$\phi_1 = \frac{-(2C_1 + C_2) + \sqrt{C_2^2 - 4C_1C_3}}{2(C_1 + C_2 + C_3)}, \quad \phi_2 = \frac{-(2C_1 + C_2) - \sqrt{C_2^2 - 4C_1C_3}}{2(C_1 + C_2 + C_3)},$$

$$B_0 = \frac{C_1 + C_2 + C_3}{C_1}, \quad B_1 = -\frac{C_2 + (C_2 + C_3)\phi_1}{C_1(\phi_1 - \phi_2)}, \quad B_2 = \frac{C_2 + (C_2 + C_3)\phi_2}{C_1(\phi_1 - \phi_2)},$$

$$D_0 = \frac{C_1 + C_2 + C_3}{C_1}w, \quad w = \frac{Q_{12}^0 - q_{12}}{Q_{12}^0}, \tag{A3.9}$$

$$D_1 = \frac{1}{C_1(\phi_1 - \phi_2)}\big[C_1 - (C_1 + C_2)w + \{C_1 - (C_1 + C_2 + C_3)w\}\phi_1\big],$$

$$D_2 = -\frac{1}{C_1(\phi_1 - \phi_2)}\big[C_1 - (C_1 + C_2)w + \{C_1 - (C_1 + C_2 + C_3)w\}\phi_2\big].$$

It should be noted that $C_2^2 - 4C_1C_3$ has a positive value for $q_{22} < Q_{22}^0$ and $q_{12} < Q_{12}^0$. Noting that $B_0 + B_1 + B_2 = D_0 + D_1 + D_2 = 1$, substitution of equations (A3.7) and (A3.8) into equation (A2.17) gives the strain response of an intact laminate for constant loading (constant stress $\bar{\sigma}_x$) as

$$\boldsymbol{\varepsilon}^0(t) = \begin{Bmatrix} 1 - B_1\left\{1 - \exp\left(\phi_1\frac{t}{T}\right)\right\} - B_2\left\{1 - \exp\left(\phi_2\frac{t}{T}\right)\right\} \\ -\left[1 - D_1\left\{1 - \exp\left(\phi_1\frac{t}{T}\right)\right\} - D_2\left\{1 - \exp\left(\phi_2\frac{t}{T}\right)\right\}\right]\nu_0 \end{Bmatrix} S_0\bar{\sigma}_x, \tag{A3.10}$$

with

$$S_0 = \frac{(b+d)(bQ_{22}^0 + dQ_{11}^0)}{(bQ_{11}^0 + dQ_{22}^0)(bQ_{22}^0 + dQ_{11}^0) - (b+d)^2(Q_{12}^0)^2},$$
$$\nu_0 = \frac{(b+d)Q_{12}^0}{bQ_{22}^0 + dQ_{11}^0}, \tag{A3.11}$$

where S_0 and ν_0 denote the initial compliance and Poisson's ratio of the laminate, respectively.

Next, the stress $\sigma_{x0}^{(2)}(t)$, which is included in equation (A2.21), is obtained from equation (A2.16) using $B_1 \gg B_2$ and $D_1 \gg D_2$ together with equation (A3.10) as

$$\begin{aligned}\sigma_{x0}^{(2)}(t) = {} & \left(Q_{22}^0 - \nu_0 Q_{12}^0\right) S_0 \bar{\sigma}_x + Q_{22}^0 \varepsilon_x^{(2)^T} + Q_{12}^0 \varepsilon_y^{(2)^T} \\ & - \Sigma_1(\bar{\sigma}_x)\left\{1 - \exp\left(-\frac{\mathrm{t}}{\mathrm{T}}\right)\right\} - \Sigma_2(\bar{\sigma}_x)\left\{1 - \exp\left(-\phi_1 \frac{t}{T}\right)\right\}, \quad \text{(A3.12)}\end{aligned}$$

with

$$\begin{aligned}\Sigma_1(\bar{\sigma}_x) = {} & q_{22}\left\{\left(1 - B_1 \frac{\phi_1}{1+\phi_1}\right) S_0 \bar{\sigma}_x + \varepsilon_x^{(2)^T}\right\} \\ & + q_{12}\left\{-\left(1 - D_1 \frac{\phi_1}{1+\phi_1}\right) \nu_0 S_0 \bar{\sigma}_x + \varepsilon_y^{(2)^T}\right\},\end{aligned}$$

$$\Sigma_2(\bar{\sigma}_x) = \left\{B_1\left(Q_{22}^0 - \frac{q_{22}}{1+\phi_1}\right) - \nu_0 D_1\left(Q_{12}^0 - \frac{q_{12}}{1+\phi_1}\right)\right\} S_0 \bar{\sigma}_x. \quad \text{(A3.13)}$$

Similarly, for linear loading at a uniform stress rate $\dot{\sigma}_x$, equation (A2.17) yields

$$\varepsilon^0(t) = \begin{Bmatrix} (1-B_1)t - \frac{B_1 T}{\phi_1}\left\{1 - \exp\left(\phi_1 \frac{t}{T}\right)\right\} - \frac{B_2 T}{\phi_2}\left\{1 - \exp\left(\phi_2 \frac{t}{T}\right)\right\} \\ -\left[(1-D_1)t - \frac{D_1 T}{\phi_1}\left\{1 - \exp\left(\phi_1 \frac{t}{T}\right)\right\} - \frac{D_2 T}{\phi_2}\left\{1 - \exp\left(\phi_2 \frac{t}{T}\right)\right\}\right]\nu_0 \end{Bmatrix} S_0 \dot{\sigma}_x. \quad \text{(A3.14)}$$

Using $B_1 \gg B_2$, $D_1 \gg D_2$ and equation (A3.14), $\sigma_{x0}^{(2)}(t)$ is given for linear loading as

$$\begin{aligned}\sigma_{x0}^{(2)}(t) = {} & Q_{22}^0 \varepsilon_x^{(2)^T} + Q_{12}^0 \varepsilon_y^{(2)^T} \\ & + \left\{(1 - B_1)\left(Q_{22}^0 - q_{22}\right) - \nu_0(1 - D_1)\left(Q_{12}^0 - q_{12}\right)\right\} S_0 \dot{\sigma}_x t \\ & + \Sigma_3\left\{1 - \exp\left(-\frac{\mathrm{t}}{\mathrm{T}}\right)\right\} - \Sigma_4\left\{1 - \exp\left(-\phi_1 \frac{t}{T}\right)\right\}, \quad \text{(A3.15)}\end{aligned}$$

with

$$\begin{aligned}\Sigma_3 = {} & q_{22}\left\{\left(1 - B_1 \frac{\phi_1}{1+\phi_1}\right) T S_0 \dot{\sigma}_x - \varepsilon_x^{(2)^T}\right\} \\ & + q_{12}\left\{-\left(1 - D_1 \frac{\phi_1}{1+\phi_1}\right) \nu_0 T S_0 \dot{\sigma}_x - \varepsilon_y^{(2)^T}\right\},\end{aligned}$$

$$\Sigma_4 = \left\{B_1\left(Q_{22}^0 - \frac{q_{22}}{1+\phi_{\ 1}}\right) - \nu_0 D_1\left(Q_{12}^0 - \frac{q_{12}}{1+\phi_1}\right)\right\} \frac{T S_0 \dot{\sigma}_x}{\phi_{\ 1}}. \quad \text{(A3.16)}$$